Control over a phase state of the laser plume ablated by femtosecond laser: Spatial pulse shaping

E. G. Gamaly, A. V. Rode, O. Uteza, V. Kolev, B. Luther-Davies, T. Bauer, J. Koch, F. Korte, and B. N. Chichkov

Citation: Journal of Applied Physics **95**, 2250 (2004); doi: 10.1063/1.1645672
View online: http://dx.doi.org/10.1063/1.1645672
View Table of Contents: http://scitation.aip.org/content/aip/journal/jap/95/5?ver=pdfcov
Published by the AIP Publishing

JOURNAL OF APPLIED PHYSICS VOLUME 95, NUMBER 5 1 MARCH 2004

Control over a phase state of the laser plume ablated by femtosecond laser: Spatial pulse shaping

E. G. Gamaly
ARC Centre for Ultra-high Bandwidth Devices for Optical Systems (CUDOS), Laser Physics Centre, Research School of Physical Sciences and Engineering, The Australian National University, Canberra, ACT 0200, Australia

A. V. Rode[a)]
Laser Physics Centre, Research School of Physical Sciences and Engineering, The Australian National University, Canberra ACT 0200, Australia

O. Uteza
Lasers, Plasma and Photonic Processes Laboratory, FRE 2165 CNRS-Aix-Marseille II University, Case 917, 163, Avenue de Luminy, 13288 Marseille Cedex 9, France, and Australian Photonics Cooperative Research Centre, Laser Physics Centre, Research School of Physical Sciences and Engineering, The Australian National University, Canberra ACT 0200, Australia

V. Kolev
Australian Photonics Cooperative Research Centre, Laser Physics Centre, Research School of Physical Sciences and Engineering, The Australian National University, Canberra ACT 0200, Australia

B. Luther-Davies
ARC Center for Ultra-high Bandwidth Devices for Optical Systems (CUDOS), and Australian Photonics Cooperative Research Centre, Laser Physics Centre, Research School of Physical Sciences and Engineering, The Australian National University, Canberra ACT 0200, Australia

T. Bauer, J. Koch, F. Korte, and B. N. Chichkov
Laser Zentrum Hannover e.V., Hollerithallee 8, D-30419 Hannover, Germany

(Received 29 September 2003; accepted 10 December 2003)

The conditions for the formation of a fully atomized laser-ablated plume using subpicosecond laser pulses have been studied theoretically and implemented experimentally. It is shown that the low-intensity wings, which generally exist in the spatial distribution of laser intensity in the focal plane and can contain a substantial part of the incident laser energy, are responsible for low-threshold phase transformations of the target and this is the major source of particulates in the ablated plume. By truncating these wings with a simple aperture and positioning the target in the image plane of that aperture, particulates can be eliminated from the plume. This is demonstrated in experiments on deposition of Si films using the truncated beam in combination with the proper choice of laser fluence. This results in an almost totally atomized plume and consequently in droplet-free deposition of thin films. © *2004 American Institute of Physics.*
[DOI: 10.1063/1.1645672]

I. INTRODUCTION

In applications of laser ablation to the deposition of thin films, or the formation of nanoclusters it is instructive to know the content and composition of the laser produced vapor or plasma. It is well known that uncontrolled contamination of the laser plume with macroscopic particles and liquid droplets is a major obstacle for many potentially attractive industrial applications of pulsed laser deposition. In this article we present a way to control the phase state of the plume, and in particular a way to achieve a fully atomized gas phase in a laser ablated plume produced by subpicosecond laser pulses.

There are a variety of processes that transform the state of a target exposed to a pulse of intense laser radiation. The major processes that appear in succession as the laser intensity increases are structural phase transitions; destruction of the target integrity (appearance of cracks, flaking of the surface); melting; ablation; and finally ionization. In what follows we determine the energy and intensity thresholds for the onset of each of these processes. These thresholds, along with the spatial and temporal intensity distribution of the laser beam allow the state of the target with increasing laser intensity to be analyzed. The analysis produces clear recommendations for the choice of the temporal and spatial distribution of laser intensity in order to achieve an efficient transformation of the target into any desired state. In particular it allows us to predict the conditions needed to produce a completely atomized vapor as is required for laser deposition of thin films with surfaces free from contamination with particles or droplets.

The dominant physical processes that occur during the interaction of intense laser radiation with matter can be di-

[a)]Author to whom correspondence should be addressed; Electronic mail: avr111@rsphy1.anu.edu.au

vided in two distinctly different regimes. The short pulse regime occurs when the pulse duration is much shorter the major relaxation times in the interaction zone, whilst in the long pulse regime the pulse duration is much longer than these relaxation times.[1] The relaxation times include the heat conduction time, t_{heat} and the electron–phonon energy exchange time, $t_{e\text{-ph}}$. Hence in the short pulse regime $t_p \ll (t_{e\text{-ph}}, t_{\text{heat}})$ and the laser energy is absorbed in a surface or skin layer of the target. The laser pulse duration typical of this short pulse regime lies in the subpicosecond range.[1–3]

In the long pulse regime the condition: $t_p \gg \{t_{\text{heat}}, t_{e\text{-ph}}\}$ is obeyed,[4,5] which occurs for laser pulse durations longer than a few picoseconds. In this regime during almost the whole interaction time, the target experiences the various transformations—amorphization, cracking, melting, and ablation—in conditions close to thermal equilibrium. The rate of these processes in equilibrium is lower than in the short pulse regime by an exponential factor. For example, the ablation (evaporation) rate $n_a \nu$ can be estimated in accordance with the Ahrrenius law to be:

$$n_a \nu \propto \exp\left(-\frac{\varepsilon_b}{kT_{\text{evap}}}\right). \tag{1}$$

Here n_a is the atomic number density of the target, ν is the velocity of the ablated vapor, ε_b is the binding energy, and kT_{evap} is the evaporation temperature. The exponential factor is small because the evaporation temperature is much smaller than the binding energy, $\varepsilon_b \gg kT_{\text{evap}}$. Since the average kinetic energy of the expanding atoms in the vapor is low, only a small number of atoms with $kT \sim \varepsilon_b$ from the high-temperature tail in the Maxwellian distribution[6] can leave a target. The time history of this adiabatic expansion, i.e., the pressure–volume ($P-V$) function, depends uniquely on the initial kinetic energy of the ablated vapor. If the initial kinetic energy of the expanding vapor is lower than a limit to be defined below (see Sec. II), the vapor inevitably enters into a state containing a mixture of phases. Formally that means that the expansion curve in a P, V plane crosses the phase equilibrium curve. By this reason the phase state of the low temperature vapor produced by thermal ablation cannot be properly controlled—it is always in a state of mixed phases.

In what follows we concentrate on the short pulse regime because it allows us to achieve better control on the phase state of the ablated plume. We introduce the thresholds for the different transformations as functions of the space and time-dependent laser intensity. Then we demonstrate that it is the laser intensity variation across the focal spot that changes the phase state of the laser plume generated from a particular point within the focal spot. A way to control the state of the plume through proper shaping of the laser pulse in space is then suggested and used in a series of experiments. In the experiments we used a top-hat like distribution created by cutting the low-intensity wings of the beam profile with a simple aperture and positioning the target into the image plane of that aperture. We show that this procedure when applied to the deposition of Si films by ablation of a Si target with 150 fs laser pulses leads to the formation of almost fully atomized plume and hence the deposition of almost particulate-free Si films. Without truncation of the beam the films are contaminated with many macroscopic particles.

II. ENERGY THRESHOLDS FOR THE PHASE TRANSITIONS

In this section we consider the laser energy density thresholds for the onset of the different phase transitions. First, we establish characteristic time and space scales for the short pulse interaction, and later we define the absorbed energy density and energy thresholds for each of the phase transitions.

A. Space and time scales in a short pulse laser–matter interaction

For short pulses (pulse duration $\ll 1$ ps) the characteristic spatial scale length where the interaction between the laser energy and the material is restricted to the laser absorption depth (or skin depth) is expressed as follows:

$$l_s = \frac{c}{\omega k}. \tag{2}$$

Here c, ω, k are the speed of light in vacuum, laser frequency, and the imaginary part of the refractive index, respectively. For metals and for semiconductors, using lasers at optical frequencies, $\omega \sim (1.5-10)\times 10^{15}$ s^{-1} the skin depth is several tens of nanometers, $l_s \sim (2-6)\times 10^{-6}$ cm. In the situation considered in this article, the average intensity in the focal spot would be expected to be in excess of 10^{14} W/cm^2. Therefore, even a semiconductor target becomes fully ionized in the first few femtoseconds of the pulse.[1] In the region where the laser energy is deposited, the electron-to-ion energy exchange time is of the order of several picoseconds.[1] In the conditions where a solid-density plasma is formed, the characteristic electron heat conduction time, that is the time for a heat wave to propagate a distance equal to the skin depth, exceeds the electron-to-ion energy exchange time. For this reason the interaction of an intense subpicosecond laser with matter falls within the short pulse interaction mode: $t_p \ll (t_{e\text{-ph}}, t_{\text{heat}})$.

B. The absorbed energy density

Since the laser field decays exponentially inside a solid in a manner analogous to the normal skin effect in metals, the spatial distribution of the temperature (or energy density) has a maximum at the target–vacuum interface. The spatial and temporal distribution of the absorbed electron energy ε_ε, calculated in the frame of the two-dimensional conventional skin effect reads:[1]

$$\varepsilon_e(r,x,t) = \frac{F(r,t)}{2n_e l_s}\exp\left\{-\frac{2x}{l_s}\right\}; \tag{3}$$

here

$$F(r,t) = \phi(r)\int_0^t A(t')I(t')dt';$$

is the laser energy density distribution (J/cm^2) absorbed in the target up to the time t; A is the dimensionless absorption

coefficient; n_e is the free-carrier density in the material; the r coordinate corresponds to the distance from the center of the circular focal spot $\phi(r)$ along the target surface, while the x coordinate is normal to the surface. We emphasise in Eq. (3) the dependence of the laser intensity on the space coordinate r across the focal spot, assuming axial symmetry in the beam. The absorbed energy in a monoatomic surface layer with thickness $d_a = n_a^{-1/3} \ll l_s$ at the end of the laser pulse reads as follows:

$$\varepsilon_e(r, d_a, t_p) n_e \approx \phi(r) \frac{A I_{\max} t_p}{2 l_s};$$

$$F(t_p) \approx A I_{\max} t_p . \tag{4}$$

Here $I_{\max}$ is the maximum intensity in the beam on the target surface. The energy defined above is a key measure for the definition of a phase transition threshold presented below.

C. Definition of phase transition threshold

We define a local threshold (that is one that depend on position within the focal spot) for any laser induced transformation of a material from the condition that the absorbed energy, defined by Eq. (4), equals the energy, $\varepsilon_{\text{transf}}$, required for the particular transformation[1]

$$\varepsilon_{\text{transf}} = \varepsilon_e \cong \frac{F(r,t)}{2 n_e l_s}. \tag{5}$$

It is obvious that the threshold energy density (fluence), $F_{\text{thr}} = A I_{\text{thr}} \times t_p \propto \varepsilon_{\text{transf}}$, scales with the characteristic energy necessary for the particular type of phase transition. For example, the ratio of ablation threshold to the melting threshold equals the ratio of the heat of vaporization H_{vap} to the heat of melting H_{melt}. This ratio varies for most of the materials in a range ~5–30. For example, for a silicon target used in the experiments below $H_{\text{vap}} = 10.6$ kJ/g; $H_{\text{melt}} = 1.66$ kJ/g;[7] and $H_{\text{vap}}/H_{\text{melt}} = 6.4$.

It is useful to start defining the ablation threshold because it directly relates to the binding energy of atom in a solid that is well known for many materials.

D. Ablation threshold

Atoms can be removed (ablated) from a solid surface if the total absorbed energy per atom exceeds the binding energy (heat of vaporization per atom) in a solid, $\varepsilon_{\text{total}} > \varepsilon_b$. Then, the ion kinetic energy comprises $\varepsilon_{\text{kin}} = \varepsilon_{\text{total}} - \varepsilon_b > 0$. During the action of the subpicosecond pulse the ions are cold $T_e \gg T_i$ because the laser pulse is shorter than the electron-to-ion energy exchange time $t_p \ll t_{\text{ei}}$. However, the ions can gain energy from the energetic electrons by means of the electrostatic field created by charge separation, or, if one ignores electron motion on the femtosecond time scale, by electron pressure.[1] Therefore, in order to ablate a material in the nonequilibrium conditions which occur for femtosecond laser pulses, the electron temperature at the solid–vapor interface must be larger than the binding energy, $T_e > \varepsilon_b$. The condition defining the local absorbed laser energy density at the distance r from the center of the focal spot for the ablation to commence then reads[1]

$$A I_{\text{thr}} t_p = F_{\text{thr}} = 2 n_e l_s (\varepsilon_b + \varepsilon_{\text{kin}}). \tag{6}$$

This condition emphasizes that the threshold energy should be significantly higher than that required to just break the interatomic bonds. Sufficient kinetic energy should be additionally delivered to an unbound atom in order to remove it from the solid and maintain it in the desired vapor state. The production of a droplet-free deposition process imposes the additional condition that the gas state of the vapor should be collisionless.

E. Criterion for total atomization of the ablated vapors

The energy threshold for total atomization of the ablated plume can be calculated on the basis of thermodynamic arguments similar to those used to derive the criterion for complete vaporization of material by strong shock waves.[8] The deposited laser energy is spent breaking the interatomic bonds and also provides the kinetic energy to the expanding plume. The magnitude of the kinetic energy sufficient to keep the expanding plume in a gaseous state containing noninteracting atoms (that is a collisionless plume), determines the absorbed energy threshold for target atomisation. Let us consider briefly the required level of laser fluence F_{atom} for the total atomization of the target material with subpicosecond laser pulses.

The target vapor experiences adiabatic expansion after the end of the pulse. Integration of the adiabatic relation, $d\varepsilon + P dV = 0$, over the volume from the initial value, V_0, corresponding to the solid state phase, up to infinity, gives a relationship between the total initial energy and the work needed to break the bonds and for vapor expansion[8]

$$\varepsilon = \varepsilon_{\text{th}} + \varepsilon_b = \int_{V_0}^{\infty} p_{\text{th}}\, dV + \int_{V_0}^{\infty} |p_b| dV . \tag{7}$$

Here p_{th} is the thermal pressure, and p_b is the pressure corresponding to the binding energy. The adiabatic expansion from a solid state to the gas state can be described with the volume-dependent Gruneisen coefficient, Γ, as follows:

$$p_{\text{th}} = p_{\text{th},0} \left(\frac{V_0}{V} \right)^{\Gamma(V)+1} . \tag{8}$$

A good approximation for Γ for metals is: $\Gamma \cong 2(V_0/V)$ at $V_0 < V < 3V_0 \cong V_{\text{cr}}$, and $\Gamma \cong 2/3$ at $V > 3V_0$.[8] Using the above reasoning we can relate the initial pressure to the pressure at a critical point via the adiabatic relation

$$p_{\text{cr}} \approx p_{\text{th},0} \left(\frac{V_0}{V_{\text{cr}}} \right)^{5/3} . \tag{9}$$

In order to get the final stage of the expansion in a gas state, the adiabatic curve in the PV plane must pass above the critical point, (p_{cr}; V_{cr}) (see Fig. 1), separating the states of a homogeneous phase from the states with a mixture of phases.[6] The critical parameters can also be expressed through the binding energy $\varepsilon_b \sim p_{\text{cr}} V_{\text{cr}}$.[8] The energy required for the adiabatic expansion of a solid with broken bonds into the collisionless gas state could be expressed through the binding energy as follows:

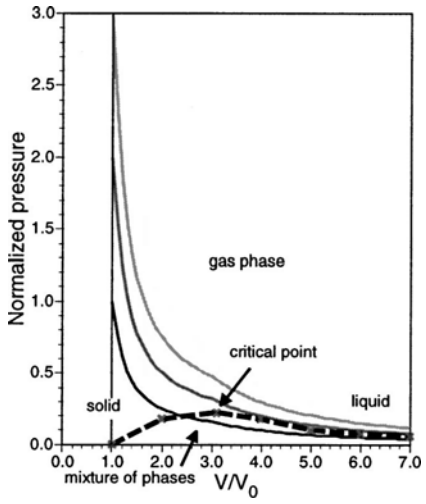

FIG. 1. $P-V$ diagram of vapor states in the plume at various levels of absorbed laser energy and thus at different initial normalized pressures. The total atomization (gas phase) is achieved at the conditions when the $P-V$ curve is above the critical point and above the curve of phase equilibrium (the Clapeyron–Clausius equation) between the mixture of phases and the gas phase (dashed curve).

$$\int_{V_0}^{\infty} p_{\mathrm{th}}\, dV \cong 1.4 p_{\mathrm{th},0} V_0 \cong \varepsilon_b \left(\frac{V_{\mathrm{cr}}}{V_0}\right)^{2/3} = 2.8\varepsilon_b ;$$

$$V_{\mathrm{cr}} \cong 3 V_0 . \tag{10}$$

Thus, the energy of approximately 3–4 times larger than the binding energy should be deposited into a solid (metal), $\varepsilon_{\mathrm{th}} \sim 3\varepsilon_b$, in order to transform the target into a fully atomized gas. We should note here that the exact value of the above numerical coefficient depends strongly on the equation of state in a range $V_0 < V < (3-5)\ V_0$ for a particular material. Therefore, the laser energy density necessary to transform the ablated material into the atomized vapor should comply with the following condition: $F_{\mathrm{atom}} > 4F_{\mathrm{thr}}$.

The dependence of normalized pressure, $P/(\varepsilon_b/V_0)$, on normalized volume (V/V_0) during the adiabatic expansion for a solid starting at the same initial density V_0^{-1} and with the different initial normalized pressure (3,2,1) is plotted at Fig. 1. The dashed curve corresponds to the states of phase equilibrium. This curve separates the states representing the mixture of phases (at $P < P_{\mathrm{crit}}$) from the states of a homogeneous phase or atomised vapors (at $P > P_{\mathrm{crit}}$). We should stress that this function is poorly known for most materials. One clearly sees from Fig. 1 that the expansion from the initial state with energy $\varepsilon > 3\varepsilon_b$ keeps the expanding vapor in a gas state while at a lower initial energy a mixture of states is unavoidable.

F. Target disintegration thresholds: Surface damage and vapor condensation

If the total deposited laser energy is close to the binding energy, $\varepsilon_{\mathrm{total}} \sim \varepsilon_b$, then the heated target experiences only a small density decrease from the normal solid density. The pressure in the material in this case is comparable to the bulk modulus. Therefore, the final state of the target affected by the laser at this energy level might be considered as "damaged," resulting in the formation of cracks, flakes, delamination of the surface, etc., depending on the presence of defects and impurities in the initial state of the target. If the deposited energy is in a range $\varepsilon_b < \varepsilon_{\mathrm{total}} < (3-4)\varepsilon_b$, then the final state of the expanding vapor may fall within a region of pressure–volume space where the mixture of phases is energetically favorable (Fig. 1). This leads to condensation of vapor into liquid droplets. We should keep in mind that the thresholds above were introduced locally, that is different regions of the beam can create different phase states depending on the local beam intensity. One should also note that the energy estimates are rather conservative (overestimated) because they are based on the assumption of thermodynamic equilibrium. In reality, and especially for short pulses, the expansion time is shorter than the equilibration time. Therefore, the expansion of vapors proceeds in the kinetic regime, and thus condensation processes are decelerated.

III. OPTIMAL PULSE PROFILE FOR ATOMIZATION OF THE PLUME

A. Temporal shape of short pulses: ASE and prepulse

The chirped pulse amplification technique[9] commonly used for the generation of energetic subpicosecond pulses often produces a prepulse containing a significant amount of energy. It is well known that to achieve the short pulse interaction mode a high contrast ratio is required between the energy of the short pulse and the prepulse. A detailed discussion of the methods for providing a high contrast ratio can be found in Ref. 3. We summarize that efficient methods to suppress the prepulse include gain narrowing; the use of the saturable absorber; and frequency conversion.

There is an additional source of the prepulse, namely, amplified spontaneous emission (ASE) from the laser amplifiers. The intensity contrast ratio of the main pulse/ASE is generally about 10^6, whilst the duration of the ASE pulse can be of 0.2–2 ns.[3,10] For example, if the prepulse associated with the ASE is of nanosecond length, $t \sim 1$ ns, and $A \sim 1$ then the intensity in the ASE prepulse of 10^8 W/cm^2 can damage the target surface before the main pulse arrives. Recently, the ASE effects on the femtosecond laser–matter interaction were revisited and it was once more confirmed that the ASE could significantly affect the interaction of a main short pulse with the target.[10] To eliminate the ASE the laser design must include successive stages of amplification interspersed with the spatial filters.[3]

B. Spatial shaping: "top-hat" spatial distribution

In order to demonstrate the importance of the spatial distribution of the laser intensity we apply the above reasoning to the problem of obtaining efficient atomization of an expanding plume produced by ablation of a material. First, we assume that the temporal pulse shape is Gaussian and the pulse is free of the ASE, prepulses, and postpulses. In most practical cases the laser intensity across the focal spot is assumed to have a Gaussian distribution with axial symmetry (beam axis is at $r=0$):

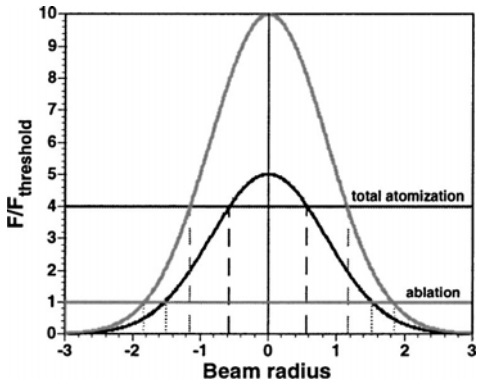

FIG. 2. Gaussian beam profile in the focal spot with the maximum fluence of $5F_{\text{thr}}$ and $10F_{\text{thr}}$. The beam radius is measured in the units of FWHM radius. The increase of maximum fluence in the beam from $5F_{\text{thr}}$ to $10F_{\text{thr}}$ improves the energy expense for total atomization from 20% to 60% and reduces the mixture of phases energy part from 60% to 30%. Accordingly, the target area producing total atomization (gas) phase in the plume is increased four times.

$$\phi(r) = \exp\left\{ -\ln 2 \frac{r^2}{r_f^2} \right\}.$$

The focal spot radius, r_f, is defined by the condition $\phi(r_f) = I/2$, i.e., the radius at the full width half maximum (FWHM) level. The part of the total energy confined in a circle of radius r is given as follows:

$$\left\{ \int_0^r \phi(r')\, \pi\, dr'^2 \right\} \left(\frac{\pi r_f^2}{\ln 2} \right)^{-1} = 1 - \exp\left\{ -\frac{r^2}{r_f^2} \ln 2 \right\}. \quad (11)$$

On the basis of the energy thresholds obtained in Sec. II and with the help of Eq. (11) one can estimate the phase state of the ablated plume for any given peak absorbed laser fluence. Choosing, for example, a laser fluence, $AI_m t_p$, five times larger than the ablation threshold (Fig. 2), one can easily calculate that only 20% of the pulse energy goes into "full atomisation" of the target material and this occurs in the beam area where $F > 4F_{\text{thr}}$ ($0 < r < 0.57 r_f$). The "mixture of phases" is produced where $F_{\text{thr}} < F < 4F_{\text{thr}}$ and this region contains ~60% of the beam energy ($0.57 r_f < r < 1.52 r_f$). The part of the beam where the "surface damage" is most probable at $F < F_{\text{thr}}$ ($r > 1.52 r_f$) consumes ~20% of the total absorbed laser energy. Therefore, the target area producing a mixture of phases in the plume is about sixfold larger than that where total atomization occurs. Thus this plume is highly likely to contain particulates or droplets and lead to the deposition of a contaminated film.

The ratio of the beam area producing a mixture of phases to that producing the fully atomized vapor can be obviously reduced by increasing the peak fluence. For example, the part of absorbed energy used up for full atomization of vapor increases three times, from 20% to 60%, if the peak absorbed fluence is increased from $5F_{\text{thr}}$ to $10F_{\text{thr}}$ (Fig. 2). Nevertheless incomplete atomisation still results.

Clearly it is very difficult to obtain complete atomization using a Gaussian beam and it is obvious that it would be preferable to use a "top-hat" intensity distribution where the absorbed fluence everywhere exceeds about four times the ablation threshold. A simple way to move towards the top-hat profile is to truncate the low energy wings in the spatial distribution with an aperture and employ a relay-imaging focusing scheme to image the top hat beam onto the target. Below we describe the experimental procedure and experiments where this idea is implemented in fs laser ablation of silicon.

IV. EXPERIMENTAL TESTS

A. Experimental conditions

A Clark-MXR CPA-2001 Ti:sapphire laser system producing 150 fs duration 775 nm pulses was used in the experiments. The laser operated at a pulse repetition rate of 1 kHz with an average power ~0.42 W at the target surface (pulse energy $E_{\text{pulse}} = 0.42$ mJ). The energy stability was typically within ±2%. As discussed earlier, a high contrast between the main pulse and any prepulse is essential to ensure operation in the ultrashort pulse interaction mode. That is the target surface should not be ionized, damaged, or ablated by the prepulse including any ASE from the laser. The ASE prepulse energy for our laser system was measured to be 12.7 μJ, and its duration ~1.0 ns, providing the laser power contrast ratio 2.2×10^5 which is sufficient for target damage by the ASE prepulse to be avoided.

The beam was delivered into the target chamber using a two-lens collimator comprising of a $f_- = -200$ mm negative lens and a $f_+ = 300$ mm focusing lens located ~925 mm apart. This combination was used to either focus the laser beam to a tight spot or image a beam shaping aperture onto the target surface to create a more top-hat like intensity distribution. The beam shaping aperture was located 1.3 m away from the negative lens and produced a ×20 demagnified image located ~3.6 mm behind the main focus of the beam. The 2.2 mm diam aperture was therefore imaged as a 110 μm disk on a target placed in the image plane. The optical scheme, together with the images of the beam on the target surface, is shown in Fig. 4 and the corresponding beam profiles in Figs. 3 and 5. The aperture transmitted ~26% of the laser energy and its size was chosen so that the absorbed fluence in the truncated spot was above the predicted threshold for total atomization of the plume (see below).

The intensity distribution in the main focus was measured by reimaging the beam onto a charge coupled device camera (Fig. 3 and Fig. 4, left hand side). The distribution was approximately Gaussian with a ~14 μm diameter (FWHM) which corresponds to a focal spot area $\sim 1.54 \times 10^{-6}$ cm^{-2}—close to the diffraction limit for the 25 mm diam input laser beam. Thus the maximum absorbed laser intensity in the focal plane was calculated to be $\sim 1.8 \times 10^{15}$ W/cm^2 and the corresponding laser fluence was 273 J/cm^2 for the 150 fs, 0.42 mJ laser pulses and assuming $A = 1$. However, these estimates are based on the assumption that the focused laser beam has an exact Gaussian profile. In reality, the intensity distribution fits a Gaussian profile only in the central area and deviates significantly from it in the low intensity wings. These wings originate from aberrations in the output beam from the laser and stray reflections and scattering from the optical surfaces in the beam path. The

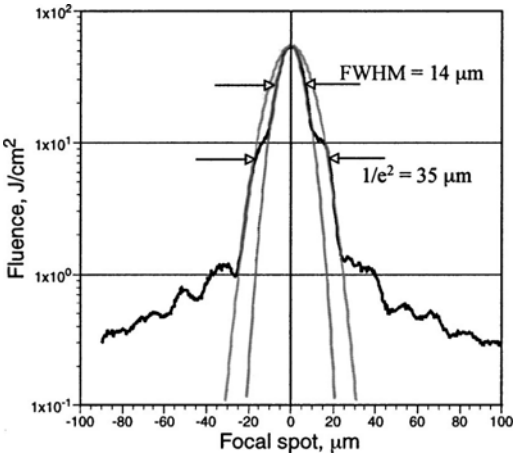

FIG. 3. Laser intensity profile in a focal spot and Gaussian fittings to the measured profile for the FWHM and $1/e^2$ intensity levels. These fits illustrate that the wings of the intensity distribution contain a substantial part, up to 30% according to our estimates, of the total beam energy. The energy in the wings is spread over much larger area around the focal spot, thus the laser intensity could be lower than the evaporation threshold but high enough to modify target material around the focal spot and to create droplets and particulates in the laser plume.

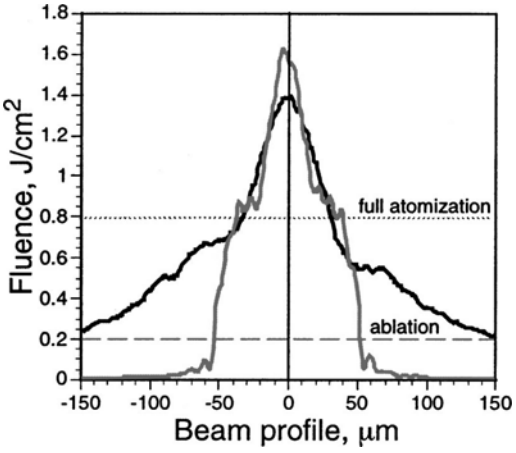

FIG. 5. Laser fluence distribution on a Si target in the 2.2 mm aperture's image plane, with opened and with closed aperture. The dashed line corresponds to the ablation threshold of $F_{\text{thr}}=0.2$ J/cm^2 for Si target, and the dotted line is the total atomization level of $4F_{\text{thr}}$.

beam profile in the focal plane shown in Fig. 3 has non-Gaussian wings containing up to 30% of the total energy of the laser pulse, and this reduced the peak fluence markedly relative to the values calculated for an ideal Gaussian beam.

To emphasis this point also shown in Fig. 3 are the profiles for Gaussian beams fitted to either the measured FWHM beam diameter (of 14 μm) or to the $1/e^2$ intensity diameter (of 35 μm). Integrating the profile to take into account the energy in the non-Gaussian wings and normalizing the result to the known energy measured using a power meter, led to a value for the maximum laser fluence in the center of the focal spot of 65 J/cm^2, corresponding to a laser intensity of 4.3×10^{14} W/cm^2—four times lower than that obtained from the estimate based on a Gaussian beam fitted at the FWHM intensity point. Thus, the Gaussian approximation significantly overestimates the laser fluence at the target surface, and therefore underestimates the affect of the low-intensity wings around the focal spot on the phase state of the laser-produced plume.

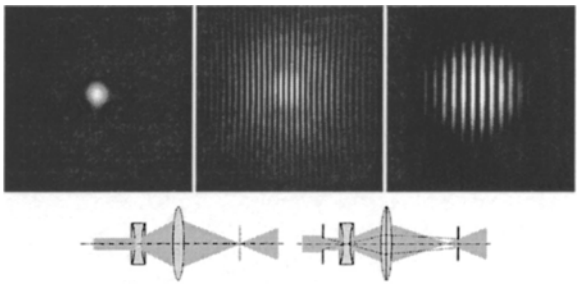

FIG. 4. The 14 μm (FWHM) focal spot (left); and the laser beam images in the imaging plane of the iris used as an aperture, with an aperture opened (center) and closed, transmitting 26.5% of the total beam energy (right). A 10 μm period reticule was placed in the image plane as a scale reference. Below the images is the two-lens optical scheme with a target in a focal plane (left) and in the aperture's image plane (right).

To try and eliminate the low intensity wings, the input beam was truncated with the aperture. The intensity distribution in the image plane without and with the aperture is shown in Fig. 4 (center and right hand side, respectively) and the intensity distributions are plotted in Fig. 5. The maximum laser fluence with the truncated beam profile was $F=1.6$ J/cm^2 ($I=1.1\times10^{13}$ W/cm^2). Removing the aperture significantly increases the laser energy delivered to the target surface, but this additional energy is mostly deposited over a large area at fluences well below the maximum value. This suggests that the best atomization conditions should be realized by using the truncated laser beam, and that a much higher density of droplets and particulates will be expected using the beam without the aperture.

To determine whether the available fluence exceeded the predicted threshold for complete atomization of the plume, knowledge of both the absorption coefficient of the target and the ablation threshold is required. To convert the measured distribution to absorbed fluence, we estimated the target absorption by measuring the ratio, R, of the energy reflected into the aperture of the focusing lens to the incoming energy finding $R_{\text{Si}}=0.36$ for $\lambda=775$ nm. Assuming then that the absorbed energy is $A=1-R$, we obtained $A_{\text{Si}}=0.64$. Measurements of the ablation threshold for Si target with 150 fs 780 nm pulses has been reported from a number of laboratories,[2,11] and the published values are in the range 0.2–0.3 J/cm^2. These values corresponded reasonably well to the estimate of 0.47 J/cm^2 based on calculations for the electrostatic regime of ablation using subpicosecond laser pulses.[1]

From Fig. 5 it is then clear that the maximum intensity in the truncated beam is up to eight times above the ablation threshold, and therefore exceeds the predicted threshold for total atomization. Hence adding the aperture should ensures that the laser produced plume is in the fully atomized state in spite of the fact that only 26% of the total laser energy is transmitted through that aperture.

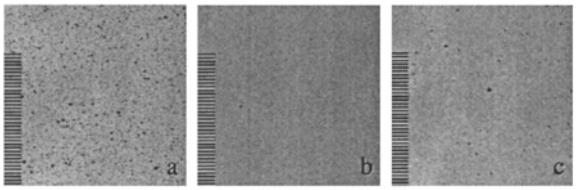

FIG. 6. Optical microscope images of Si film surfaces deposited with the different focusing conditions of the same laser beam: (a) target is in the focal spot; the density of droplets is $>1000\ \mathrm{cm}^{-2}$; (b) target is in the image plane of a 2.2 mm iris with ×20 demagnification; the density of droplets is reduced to $\sim 10\ \mathrm{cm}^{-2}$; and (c) target is in the same image plane as in (b), the iris is open; the droplets density increases to $\sim 100\ \mathrm{cm}^{-2}$. A 10 μm scale is presented on the left border of each image.

B. Experimental results on Si-film depositions

A Si wafer was used as a target in a vacuum chamber where the base pressure was kept at the level $(0.7-1.2)\times 10^{-6}$ Torr. The laser beam was scanned over a $1\times 1\ \mathrm{cm}^2$ area of the target surface with a dual-axis galvanometer scanning system forming a rectangular-shaped ablated zone. The mirror scanning speed was about 50 Hz in both x and y axes in order to guarantee a single laser shot per site and to avoid overlapping of two consecutive pulses on the target surface. Fused silica substrates were located at a distance 60 mm from the target. The deposition rate measured with a quartz microbalance thickness monitor was at the level 0.25–0.5 Å/s, higher at the beginning of the deposition and slowing down due to the darkening of the entrance window during the deposition. The thickness of the films deposited for the droplets and particulates density postanalysis was in the range 85–100 nm over the substrate surface; and a typical deposition time was around 1 h.

There were three series of experiments conducted: with the target located at the focal spot at the maximum intensity; with the target located at the image plane of the 2.2 mm diam aperture; and at the same target position but with the aperture removed. Optical micrographs of the resulting films are shown in Fig. 6.

The analysis of these optical images revealed that the density of 1–10 μm droplets on the substrate surface was above $1000\ \mathrm{cm}^{-2}$ [Fig. 5(a)] when the target was positioned in the focal plane where the absorbed laser fluence was $\mathrm{AF}=65\ \mathrm{J/cm^2}\times 0.64=41.6\ \mathrm{J/cm^2}$ ($I_{\mathrm{abs}}=2.8\times 10^{14}\ \mathrm{W/cm^2}$). By placing the target in the image plane of the aperture the maximum fluence of the truncated beam was reduced to $\mathrm{AF}=1.6\ \mathrm{J/cm^2}\times 0.64=1\ \mathrm{J/cm^2}$ ($I_{\mathrm{abs}}=6.8\times 10^{12}\ \mathrm{W/cm^2}$). This eliminated droplets almost totally from the deposited Si film: the density of droplets was reduced to below $10\ \mathrm{cm}^{-2}$ [Fig. 5(b)]. In order to test the influence of low-intensity wings in the spatial pulse profile on the droplet formation, another deposition was performed with the target in the same position but with the aperture removed. The density of droplets then increased to above $100\ \mathrm{cm}^2$ [Fig. 5(c)]. This experiment provided a clear demonstration that the low intensity wings in the spatial distribution are responsible for the formation of droplets on the deposited film surface.

Positioning the target in the image of the aperture may also eliminate the problem of droplet formation by any the prepulse. The effect of the prepulse could be estimated in the following way. The measured 1 ns prepulse containing 12.7 μJ results at most in $5.4\times 10^7\ \mathrm{W/cm^2}$ absorbed laser intensity in the target before the arrival of the main pulse. The depth of the heat wave propagation, l_{heat} can be estimated as $l_{\mathrm{heat}}=\sqrt{at_{p-p}}$; here a is thermal diffusivity ($a_{\mathrm{Si}}=0.85\ \mathrm{cm^2\ s^{-1}}$)[7] and t_{p-p} is the prepulse duration, thus $l_{\mathrm{heat}}=0.29\ \mu$m. This leads to the maximum absorbed energy in the heated volume below the target surface of 1.26×10^3 J/g. This value is below the heat of melting of 1.66×10^3 J/g for Si,[7] thus the prepulse could not melt the target in the focal spot before the arrival of the main subpicosecond pulse. However, the energy of the prepulse would still be high enough to cause some material transformation such as for example, the formation of cracks, which may be the reason for the presence of a small number of micron-size particles on the deposited film shown in Fig. 5(b).

V. DISCUSSION AND CONCLUSION

We have formulated the local thresholds for the different material transformations under the action of short powerful laser pulses. In particular, we obtained the energy conditions required to achieve a fully atomized gas phase in the laser-ablated plume produced by subpicosecond laser pulses.

The crucial role of the spatial distribution of the laser intensity across the focal spot on the phase state of the ablated plume has been demonstrated. The low-intensity wings in the spatial distribution of the laser intensity contain a substantial part of the incident laser energy. The low-intensity area is responsible for the low-threshold material transformations, such as amorphization, surface damage, and melting. These transformations produce a mixture of phases in the laser plume such as liquid droplets, flakes, and micron-size particles. It is these low-intensity parts of the laser beam that lead to poor quality of the deposited films.

A way of controlling the phase state of the plume by shaping of the focused beam at the target was suggested and implemented in the series of experiments. A good approximation to the ideal top-hat-like spatial distribution can be achieved by truncating the original Gaussian-like beam with a simple aperture and positioning the target in the image plane of that aperture using an appropriate optical system. The experimental implementation of his procedure led to almost fully atomized plume and to a deposition of almost droplet-free thin films.

ACKNOWLEDGMENTS

E.G.G. and A.V.R. gratefully acknowledge financial support from the Australian–German Joint Research Cooperation Scheme. O.U. gratefully acknowledges Australian Research Council's financial support through the ARC-IREX scheme (Grant No. X00106527 "Ultrafast laser ablation and deposition of thin films"). This work was produced with the assistance of the ARC Centres of Excellence program. CUDOS (the Center for Ultrahigh bandwidth Devices for Optical Systems) is an ARC Center of Excellence.

[1] E. G. Gamaly, A. V. Rode, V. T. Tikhonchuk, and B. Luther-Davies, Phys. Plasmas **9**, 949 (2002).
[2] J. Bonse, S. Baudach, J. Kruger, W. Kautek, and M. Lenzner, Appl. Phys. A: Mater. Sci. Process. **74**, 19 (2002).
[3] B. Luther-Davies, E. G. Gamaly, Y. Wang, A. V. Rode, and V. T. Tikhonchuk, Sov. J. Quantum Electron. **22**, 289 (1992).
[4] Yu. V. Afanasiev and O. N. Krokhin, in *Physics of High Energy Density*, edited by P. Calderola and H. Knoepfel (Academic, New York, 1971).
[5] S. I. Anisimov, Y. A. Imas, G. S. Romanov, and Yu. V. Khodyko, *Action of High-Power Radiation on Metals* (Consultant Bureau, Springfield, 1971).
[6] L. D. Landau and E. M. Lifshitz, *Statistical Physics*, Part 1 (Pergamon, Oxford, 1960).
[7] *CRC Handbook of Chemistry and Physics, 60th* ed., edited by R. C. Weast and M. J. Astle (CRC, Boca Raton, 1981).
[8] Ya. B. Zel'dovich and Yu. P. Raizer, *Physics of Shock Waves and High-Temperature Hydrodynamic Phenomena* (Dover, Mineola, 2002).
[9] P. Maine, D. Strickland, P. Bado, M. Pessot, and G. Mourou, IEEE J. Quantum Electron. **24**, 398 (1988).
[10] K. B. Wharton, C. D. Boley, A. M. Komashko, A. M. Rubenchik, J. Zweiback, J. Crane, G. Hays, T. E. Cowan, and T. Ditmire, Phys. Rev. E **64**, 025401 (2001).
[11] P. P. Pronko, P. A. VanRompay, C. Horvath, F. Loesel, T. Juhasz, X. Liu, and G. Mourou, Phys. Rev. B **58**, 2387 (1998).